ACS APPLIED MATERIALS & INTERFACES

www.acsami.org

Research Article

Heteroepitaxy of Large-Area, Monocrystalline Lead Halide Perovskite Films on Gallium Arsenide

Deying Kong, Yu Zhang, Dali Cheng, Enze Wang, Kaiyuan Zhang, Huachun Wang, Kai Liu, Lan Yin,* and Xing Sheng*

Cite This: *ACS Appl. Mater. Interfaces* 2022, 14, 52508−52515

Read Online

ACCESS | Metrics & More | Article Recommendations | Supporting Information

ABSTRACT: Lead halide perovskite materials have been emerging as promising candidates for high-performance optoelectronic devices. Significant efforts have sought to realize monocrystalline perovskite films on a large scale. Here, we epitaxially grow monocrystalline methylammonium lead tribromide ($MAPbBr_3$) films on lattice-matched gallium arsenide (GaAs) substrates on a centimeter scale. In particular, a solution-processed lead(II) sulfide (PbS) layer provides a lattice-matched and chemical protective interface for the solid−gas reaction to form $MAPbBr_3$ films on GaAs. Structure characterizations identify the crystal orientations in the trilayer $MAPbBr_3$/PbS/GaAs epistructure and confirm the monocrystalline nature of $MAPbBr_3$ on PbS/GaAs. The dynamic evolution of surface morphologies during the growth indicates a two-step epitaxial process. These fundamental understandings and practical growth techniques offer a viable guideline to approach high-quality perovskite films for previously inaccessible applications.

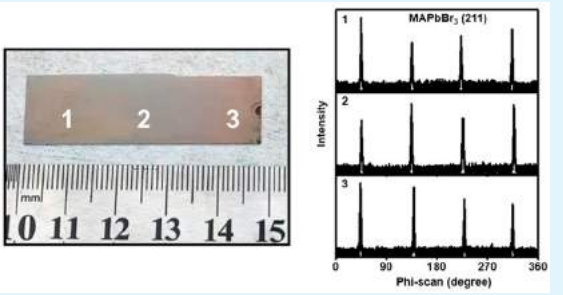

KEYWORDS: *lead halide perovskite, epitaxy, single crystal, gallium arsenide, lead sulfide*

1. INTRODUCTION

In the past few years, hybrid lead halide perovskites have become promising candidates as new-generation semiconductors for advanced optoelectronic materials and devices, including remarkable developments like high-efficiency solar cells and light-emitting diodes (LEDs).[1−5] In spite of these achievements, these devices are mostly based on polycrystalline perovskites, and it is imperative to obtain large-area, single-crystalline perovskite films with a high quality on par with traditional semiconductors like silicon (Si) or gallium arsenide (GaAs).[6−9] Certain accomplishments have been achieved,[10] for example, by growing monocrystalline perovskite films via lattice-matched homoepitaxy or metamorphic heteroepitaxy on uncommon substrates like monocrystalline perovskites,[11−14] metal halides,[15,16] or lead chalcogenides.[17,18] Other attempts include the growth of perovskite crystals on more common but lattice-mismatched substrates like Si, GaN, quartz, gold, sapphire, mica, etc.,[18−27] via spin coating, inkjet printing, mechanical slicing, space-confined crystallization, chemical vapor deposition, electrodeposition, etc.[21,23,24,28−30] However, crystal sizes formed on these lattice-mismatched substrates are limited to scales ranging from several micrometers to several millimeters. In a word, existing approaches either require lattice-matched crystals that are not readily available, or utilize lattice-mismatched substrates that constrain the growth of large-area, monocrystalline perovskite films. In other words, the limited availability of large-area, lattice-matched substrates and their associated growth strategies hinder the formation of large-area, monocrystalline perovskite films, which has long been desired for unprecedented device applications.

2. RESULTS AND DISCUSSION

In this work, we report the epitaxial growth of centimeter-scale, monocrystalline methylammonium lead tribromide ($CH_3NH_3PbBr_3$, or $MAPbBr_3$) perovskite films on lattice-matched GaAs wafers. Coincidentally, cubic-phase $MAPbBr_3$ has a lattice constant (a = 5.91 Å)[31] close to that of zinc-blende GaAs (a = 5.65 Å), making the lattice-matched or metamorphic epitaxy possible. To evaluate this hypothesis, we first attempt to grow $MAPbBr_3$ via conventional chemical vapor deposition (CVD),[32] following the reaction of methylammonium bromide (CH_3NH_3Br, or MABr) and lead(II) bromide ($PbBr_2$) at 350 °C (Figure S1a):

$$CH_3NH_3Br(g) + PbBr_2(g) = CH_3NH_3PbBr_3(s) \quad (1)$$

This reaction produces polycrystalline $MAPbBr_3$ on lattice-mismatched Si (100) substrates (a = 5.43 Å) (Figure S1b), which is expected and in accordance with previous reports.[32]

Received: August 26, 2022
Accepted: October 31, 2022
Published: November 9, 2022

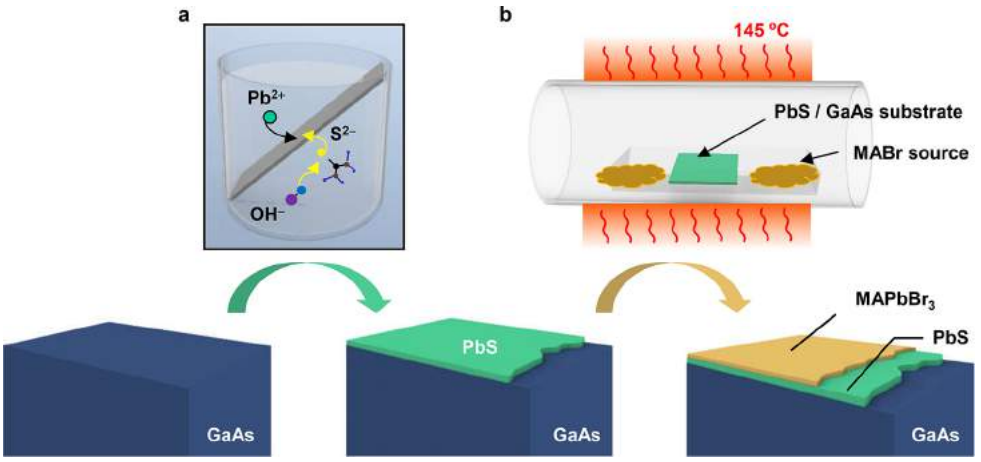

Figure 1. Schematic illustration of the $MAPbBr_3$ epitaxy on GaAs. (a) Single-crystalline PbS film is grown on GaAs via chemical bath deposition. (b) PbS film then reacts with MABr in a chemical vapor deposition tube to form a single-crystalline $MAPbBr_3$ film.

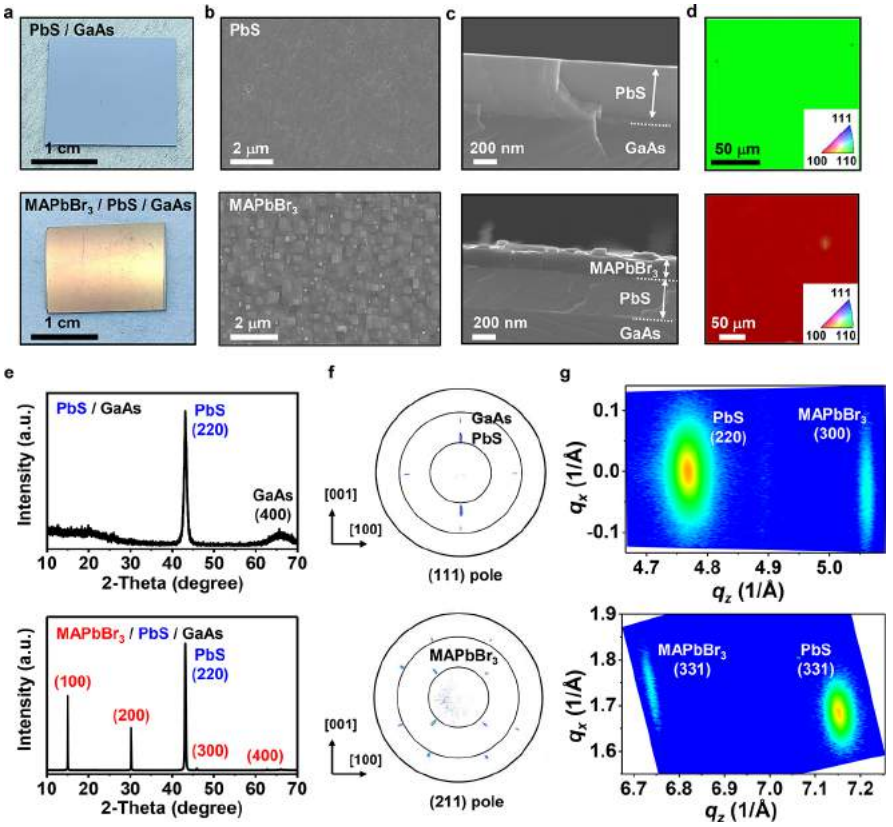

Figure 2. Structural characterizations for PbS-on-GaAs and $MAPbBr_3$-on-PbS-on-GaAs samples. (a) Top-view photographs, (b) top-view SEM images, (c) cross-sectional SEM images, (d) EBSD maps, (e) XRD patterns, and (f) pole figures for two samples (top, PbS/GaAs; bottom, $MAPbBr_3$/PbS/GaAs). (g) RSMs around (300) and (331) points of $MAPbBr_3$.

However, the same synthesis process results in the formation of lead (Pb) powders on GaAs (100), which makes the direct CVD growth of $MAPbBr_3$ unsuccessful (Figure S1c). This observation is likely to be attributed to more favorable reactions between bromides and GaAs at 350 °C, which is widely applied in the GaAs dry etching process.[33,34] Since the Ga−Br bond has a higher bonding energy than that of the Pb−Br bond,[35] the reaction could dissociate $PbBr_2$ to form Pb solids as well as volatile byproducts like gallium(III) bromide ($GaBr_3$) and arsenic tribromide ($AsBr_3$). In fact, many group III and group V halides form volatile gases (for example, boiling points are 201 °C for $GaCl_3$, 130 °C for $AsCl_3$, 173 °C for PBr_3, etc.). Therefore, even if the lattice matching requirement is satisfied, such detrimental processes could prevent the direct epitaxy of various halide perovskites on GaAs at elevated temperatures.

To bypass this challenge, we introduce a lead(II) sulfide (PbS) interface layer to ameliorate the epitaxial growth of $MAPbBr_3$ on GaAs (Figure 1). The PbS layer is grown on GaAs via chemical bath deposition (CBD) by the reaction of lead and sulfur ions in the alkaline solution (Figure 1a):

$$Pb^{2+}(aq) + S^{2-}(aq) = PbS(s) \quad (2)$$

https://doi.org/10.1021/acsami.2c15243
ACS Appl. Mater. Interfaces 2022, 14, 52508−52515

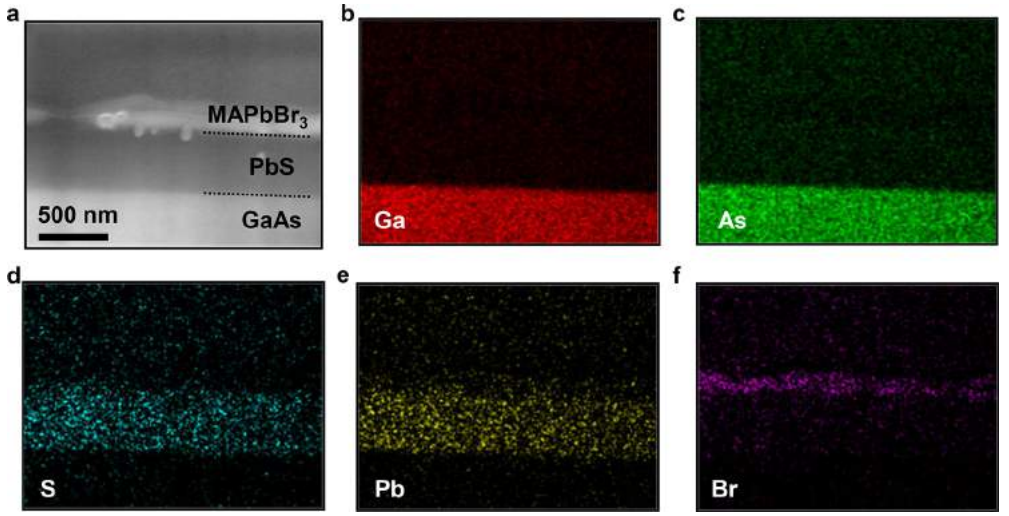

Figure 3. (a) Cross-sectional SEM image and (b–f) corresponding energy-dispersive X-ray spectroscopy (EDS) element mappings for the $MAPbBr_3$/PbS/GaAs sample.

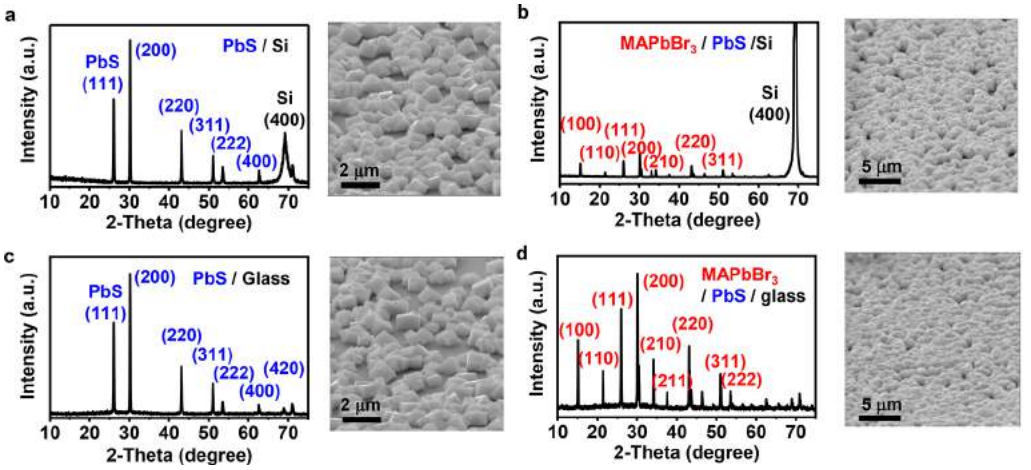

Figure 4. Structural characterizations of PbS and $MAPbBr_3$ films grown on Si and glass substrates via the same process as in Figure 1. XRD patterns (left) and SEM images (right) for (a) PbS on Si, (b) $MAPbBr_3$ on PbS/Si, (c) PbS on glass, and (d) $MAPbBr_3$ on PbS/glass. All these films are polycrystalline.

The alkaline solution helps eliminate the native oxide on GaAs and facilitate the epitaxial process to form monocrystalline PbS (Figure S2).[36,37] Subsequently, the $MAPbBr_3$ film is formed by the solid–gas reaction between MABr and PbS in the CVD tube at 145 °C (Figure 1b):

$$3CH_3NH_3Br(g) + PbS(s) = CH_3NH_3PbBr_3(s) + 2CH_3NH_2(g) + H_2S(g) \quad (3)$$

Similar reactions were previously employed to form perovskite-based ($MAPbI_3$) nanocrystals or quantum dots[38−42] but have not been explored to form large-area monocrystalline perovskite films. The introduction of the PbS interlayer is advantageous in multiple aspects: (1) PbS has a face-centered cubic (FCC), rock salt structure almost perfectly lattice-matched (a = 5.93 Å) to $MAPbBr_3$, working as an ideal buffer layer between $MAPbBr_3$ (a = 5.91 Å) and GaAs (a = 5.65 Å); (2) PbS protects GaAs against detrimental reactions with halides; (3) PbS serves as a Pb source and directly reacts with MABr, reducing the CVD temperature from 350 to 145 °C. Such material choices and process strategies eventually cause the formation of a large-area, monocrystalline $MAPbBr_3$ film on GaAs, which is systematically analyzed subsequently.

Figure 2 presents materials and crystal characterizations for the PbS/GaAs and the $MAPbBr_3$/PbS/GaAs epitaxial structures. Figure 2a, b show that both the PbS and the $MAPbBr_3$ films form uniform coatings on a GaAs (100) wafer sample with a dimension of around 2 × 2 cm^2. Flaws in the edge and on the sample surface are mostly due to the uncleaned sample surface and particles in the CBD growth solution and the CVD chamber. In addition, the $MAPbBr_3$ film presents a highly ordered island structure with cube-shaped crystals all oriented along the cleavage directions ([110] and [1$\bar{1}$0]) of GaAs (100) wafers (Figure 2b, bottom). Cross-sectional scanning electron microscopic (SEM) images (Figure 2c) and corresponding energy-dispersive X-ray spectroscopy (EDS) element mappings (Figure 3) indicate that the as-prepared PbS film has a thickness of ∼500 nm after ∼5 min CBD, and the $MAPbBr_3$ layer is ∼200 nm thick after ∼8 h CVD. Electron back scatter diffraction (EBSD) mappings (Figure 2d) clearly illustrate that both the PbS and the $MAPbBr_3$ films have monocrystalline characteristics, with a preferential growth in [110] and [100] directions, respectively.

https://doi.org/10.1021/acsami.2c15243
ACS Appl. Mater. Interfaces 2022, 14, 52508−52515

In agreement with EBSD data, out-of-plane X-ray diffraction (XRD) patterns in Figure 2e confirm that the PbS and the $MAPbBr_3$ films have growth planes of (220) and (100), respectively. After reaction, the $MAPbBr_3$ film contains minimal traces of sulfur residues with XRD and EDS signals below the background noise level. For comparison, the same procedures to grow PbS and $MAPbBr_3$ films are performed on Si and glass substrates. As expected, XRD results indicate that these films are polycrystalline on Si and glass (Figure 4). Additionally, the PbS/GaAs and the $MAPbBr_3$/PbS/GaAs samples are characterized by Rutherford backscattering spectrometry.[43] At the channeling condition (under helium ion beams normal to the film plane), the backscattered ion yields for both samples are notably less than the nonchanneling condition (when samples are tilted by 2°), suggesting well-ordered crystal planes for these epitaxial films (Figure 5).

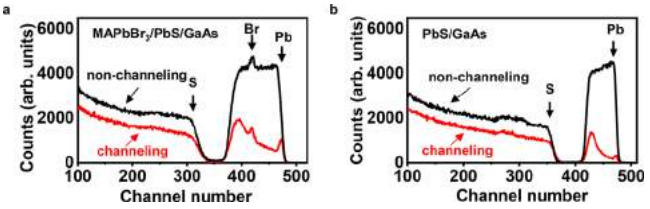

Figure 5. Rutherford backscattering spectra (RBS) at channeling (normal incidence) and nonchanneling (2° tilted orientation) conditions for two samples: (a) $MAPbBr_3$ on PbS/GaAs and (b) PbS on GaAs. The ion source is 2 MeV $^4He^+$.

Pole figures in Figure 2f further elucidate in-plane orientations for PbS and $MAPbBr_3$ crystalline films. The (111) pole figure of PbS with two spots separated azimuthally by 180° at a tilt angle of 35°, corresponding to the angle between (111) and (220) planes, indicates the in-plane orientation of PbS with respect to GaAs (Figure 2f, top). Additionally, the (211) pole figure of $MAPbBr_3$ shows four spots separated azimuthally by 90° at a tilt angle of 35°, corresponding to the angle between (211) and (100) planes, and eight spots that are divided into two identical rectangular patterns, indicating the 4-fold symmetry of the (100) plane. Moreover, the four spots at 35° and eight spots at 66° are results of (211) and (112) planar reflections.[44] It is noted that the (211) planes are unique for simple-cubic perovskite $MAPbBr_3$ and do not present in the rock salt structure of PbS or the zinc-blende GaAs. The (211) patterns of $MAPbBr_3$ rotate by 45° in plane in relation to GaAs [100] direction, indicating the orientation of the $MAPbBr_3$ crystal. The clearly distinct spot patterns with a low background noise reveal the high quality of monocrystalline PbS and $MAPbBr_3$ films. Results of reciprocal space mapping (RSM) analysis are obtained around (300) and (331) points of $MAPbBr_3$ (Figure 2g). The asymmetric feature suggests the existence of different in-plane strains in different directions. Collectively, these experimental results clearly demonstrate the single crystal feature of the $MAPbBr_3$ film epitaxially formed on the PbS/GaAs substrate.

Monocrystalline GaAs (100) substrates have been extensively used in optoelectronic industry at affordable costs up to 8 in. in diameter.[45] Its widespread availability promises the potential to scale up the heteroepitaxy of $MAPbBr_3$ films. Figure 6a presents a $MAPbBr_3$/PbS/GaAs sample with a size of 1.5 × 5 cm^2, in which three different locations are independently examined with SEM and XRD. Here we perform in-plane phi scanning on the (211) plane of the $MAPbBr_3$ film since it is unique for the simple

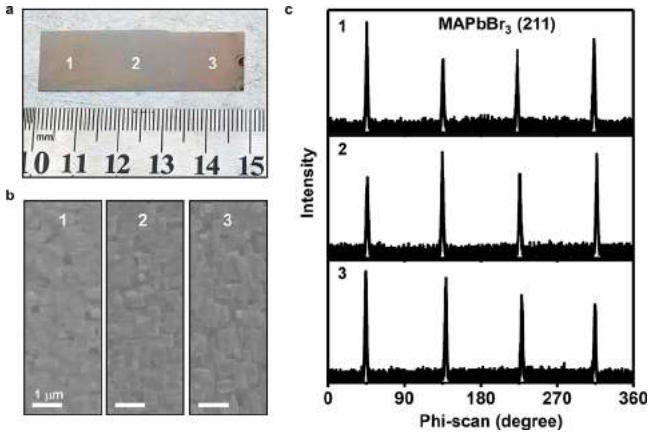

Figure 6. Large-area single-crystalline $MAPbBr_3$ film on PbS/GaAs. (a) Photograph of the sample with dimensions of 1.5 × 5 cm^2. (b) Top-view SEM images at three different locations. (c) XRD phi-scan patterns of the $MAPbBr_3$ (211) plane at three different locations.

cubic perovskite structure and will not be interfered by PbS or GaAs. The surface topology and roughness are similar in different regions across the entire sample (Figure 6b), and consistent XRD peaks of the (211) plane during in-plane phi scanning reveal the single-crystal phase forming across the entire sample surface.

Based on the XRD results obtained in Figure 2, we established a 3D atomic scheme to interpret the $MAPbBr_3$/PbS/GaAs epistructure, illustrated in Figure 7. This illustration is based on crystal orientations deduced by X-ray characterization, and consistent with the perovskite/PbS and PbS/GaAs interfacial structures described in previous reports.[46,47] According to Figure 2d–f, the epitaxial relation is $MAPbBr_3$ (100) ∥ PbS (110) ∥ GaAs (100), $MAPbBr_3$ [001] ∥ PbS [001] ∥ GaAs [011], and $MAPbBr_3$ [010] ∥ PbS [$1\bar{1}0$] ∥ GaAs [$01\bar{1}$]. Specifically, the PbS layer grows up along its [110] direction on GaAs (100), and in-plane directions [001] and [$1\bar{1}0$]are parallel to GaAs [011] and [$01\bar{1}$], respectively. This observation is consistent with previous reports.[47] While there is only an ∼5% mismatch between PbS [$1\bar{1}0$] and GaAs [$01\bar{1}$], the mismatch between PbS [001] and GaAs [011] is as large as ∼50%. Therefore, the lattice registry is most likely metamorphic along GaAs [$01\bar{1}$] and coincident along GaAs [011], forming a structure with 3 GaAs and 2 PbS, with a mismatch of ∼1.2%. Similar observations are obtained at the $MAPbBr_3$/PbS heterointerface. The lattice is almost perfectly matched between $MAPbBr_3$ [001] and PbS [001], but there is an ∼50% mismatch between $MAPbBr_3$ [010] and PbS [$1\bar{1}0$]. Therefore, the coincident growth along PbS [$\bar{1}10$] creates a structure with 3 PbS and 2 $MAPbBr_3$, with a mismatch of ∼5%. It should be noted, however, the exact atomic configurations at both interfaces are currently unknown and sketches here are speculative. Detailed structures at the interfaces, including dislocations, film strains, defects, etc., can be further analyzed experimentally and theoretically, using XRD peak shift, confocal spectroscopy, and first-principle simulations in the future. Mechanisms for such a growth preference remain unclear, which are probably ascribed to the different crystal structures of GaAs (zinc blende), PbS (rock salt), and $MAPbBr_3$ (perovskite).

The epitaxial process for $MAPbBr_3$ on PbS/GaAs is further investigated by examining the film morphology with SEM and atomic force microscopy (AFM), at different time courses during the growth (Figure 8). The as-grown PbS/GaAs sample

https://doi.org/10.1021/acsami.2c15243
ACS Appl. Mater. Interfaces 2022, 14, 52508−52515

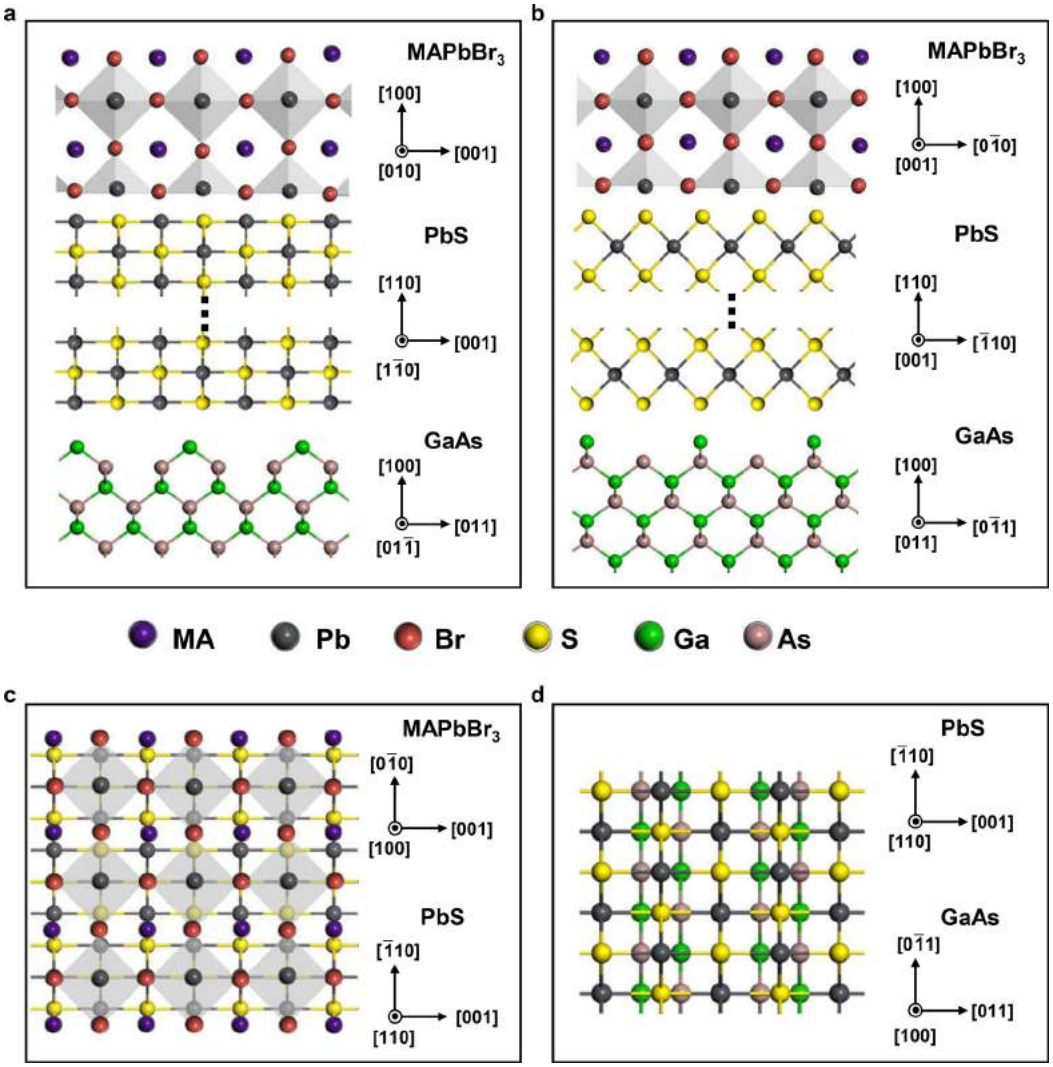

Figure 7. Conceptual illustration of the $MAPbBr_3$/PbS/GaAs epitaxial structure. (a) Side view normal to the PbS [110] direction. (b) Side view normal to the PbS [001] direction. (c) Top view of the stacked $MAPbBr_3$ (100)/PbS (220) heterointerface. (d) Top view of the stacked PbS (220)/GaAs (100) heterointerface.

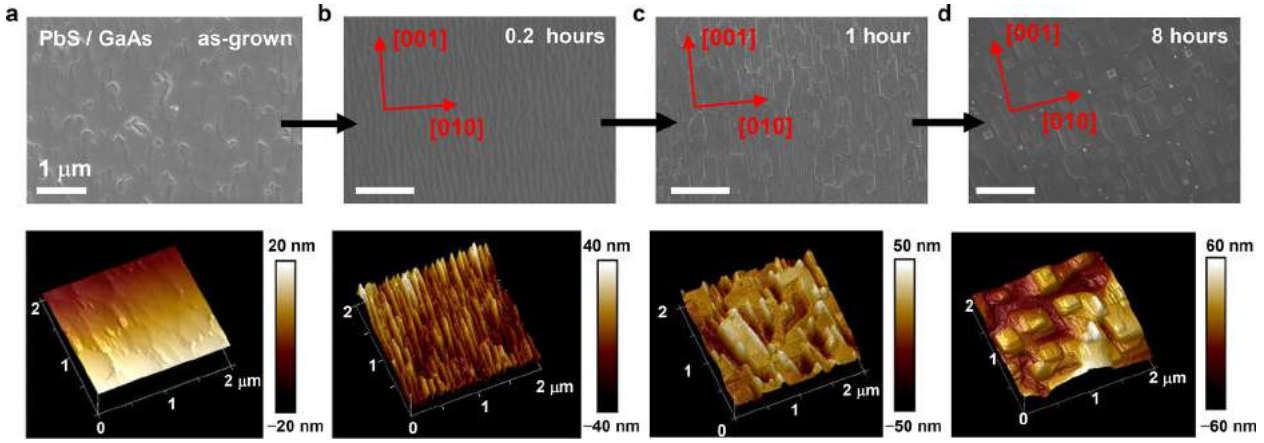

Figure 8. Evolution of surface morphology during the $MAPbBr_3$ epitaxy on PbS/GaAs. SEM (top) and AFM (bottom) images for (a) the as-grown PbS/GaAs sample, and after growth for (b) 0.2 h, (c) 1 h, and (d) 8 h. Arrows indicate the crystal directions of $MAPbBr_3$.

has a root-mean-square (RMS) roughness of ~5.4 nm (Figure 8a). Observed surface defects are likely related to misfit dislocations. Clearly, the growth of $MAPbBr_3$ on PbS/GaAs divides into two distinct steps. In the first step, the solid−gas reaction of MABr and PbS occurs on the PbS surface. The reaction is similar to a previous work reporting the transformation of a PbS polycrystalline film to a polycrystalline perovskite ($MAPbI_3$) layer.[38] After CVD growth for 0.2 h, a

https://doi.org/10.1021/acsami.2c15243
ACS Appl. Mater. Interfaces 2022, 14, 52508−52515

$MAPbBr_3$ film appears and forms an undulating surface with a period of ~70 nm and an RMS roughness of ~8.5 nm (Figure 8b). In particular, the striped structures follow the cleavage directions of GaAs (100) wafers, which are [110] and [1$\bar{1}$0]. Such an anisotropic growth can be explained by the lattice matching conditions between $MAPbBr_3$ and PbS, which results in distinct appearance along the two in-plane directions [001] and [010] for $MAPbBr_3$ (Figure 7). The mechanisms are analogous to the classical Frank−van der Merwe growth in the $MAPbBr_3$ [001] direction, and the Volmer−Weber growth in the $MAPbBr_3$ [010] direction.[48] As the process continues, the MABr gas has to diffuse through the $MAPbBr_3$ film and reacts with the PbS underneath it. The second step forms more rectangular or cubic-shaped $MAPbBr_3$ crystals and eventually results in a continuous film surface with terrace morphology (Figure 8c, d). After CVD growth for 8 h, the $MAPbBr_3$ film has an RMS roughness of ~12.6 nm. The maximum roughness (R_{max}) is approximately 100 nm and roughness curve is shown in Figure S3. It is noted that the $MAPbBr_3$ growth rate considerably decreases as the film becomes thicker, since the film growth is eventually limited by the diffusion of MABr gas into the $MAPbBr_3$ film. We do not observe a thickness increase for the $MAPbBr_3$ film from 8 to 24 h. During this process, the PbS single-crystal film serves as a lattice-anchored substrate.[49] Such growth kinetics is analogous to the thermal oxidation of silicon.[50]

3. CONCLUSION

In summary, we demonstrate the heteroepitaxy of centimeter-scale, monocrystalline $MAPbBr_3$ films on GaAs (100) via the gas−solid reaction, with a solution-processed PbS interfacial layer. Such a growth strategy overcomes the limitations of previously explored methods, and heterogeneously integrates an emerging lead halide perovskite material with a traditional III−V compound semiconductor, in a single-crystal format. The applied CBD and CVD processes, as well as the use of GaAs (100) wafers, are compatible with large-scale manufacturing. It is envisioned that these concepts could immediately realize high-quality monocrystalline perovskites on 6 in. and even 8 in. GaAs wafers. Future possibilities involve the large-area production of many other halide perovskites with similar lattice structures, for example, $MAPbCl_3$ (a = 5.67 Å), $CsPbCl_3$ (a = 5.61 Å), and $CsPbBr_3$ (a = 5.87 Å). These monocrystalline materials could potentially produce perovskite-based optoelectronic devices with higher performance, although additional issues associated with device design and fabrications must be considered. Preliminary photoluminescence tests show that the monocrystalline $MAPbBr_3$/PbS/GaAs structure shows a lower PL peak intensity than the polycrystalline $MAPbBr_3$/PbS/glass sample (Figure S4), mainly due to the high-index and absorptive GaAs substrate. In addition, the band alignments and electron/photon couple at the interfaces in the perovskite/PbS/GaAs trilayer structure should be systematically investigated, which require additional efforts in the future. Furthermore, structure and performance stability is also a critical issue for halide perovskites,[51] and additional coatings could be applied and optimized on the $MAPbBr_3$ surface to mitigate its degradation with moisture. Collectively, the concepts provide a promising direction for fundamental materials research and advanced device applications.

4. EXPERIMENTAL METHODS

PbS Growth. PbS films are grown on GaAs (100) wafers (single-side polished, updoped, AXT Inc.) via chemical bath deposition (CBD) at 50 °C in ambient environment (Figure 1a). The GaAs substrates are cleaved into rectangular pieces with a diamond pen. The chemical solution contains 270 mM sodium hydroxide (NaOH powder, 97%, Alfa Aesar), 10 mM lead nitrate ($Pb(NO_3)_2$ powder, 99.99%, Aladdin) and 50 mM thiourea ($SC(NH_2)_2$ powder, 99%, Sigma-Aldrich). The growth rate is ~1 nm/s. The polished side of GaAs faces down in the solution, to avoid PbS cluster particles randomly falling on the growth surface. The PbS deposition is also performed on Si (100) wafers and glass substrates for comparison.

$MAPbBr_3$ Growth on PbS/GaAs. $MAPbBr_3$ films are formed on PbS/GaAs substrates via chemical vapor deposition (CVD) with a solid−gas reaction (Figure 1b). As-grown PbS/GaAs samples and excessive (~1 g) methylammonium hydrobromide (MABr powder, 98%, TCI Chemicals) are placed in a quartz tube furnace (OTF-1200X-S, tube diameter 50 mm, MTI Corp.) The reaction of MABr and PbS to form $MAPbBr_3$ occurs at 145 °C in an argon environment at a pressure of ~100 Pa. The $MAPbBr_3$ growth is also performed on PbS/Si and PbS/glass substrates for comparison.

$MAPbBr_3$ Growth on Si and GaAs. $MAPbBr_3$ growth is also attempted on Si and GaAs substrates via traditional CVD methods[32] without the PbS interlayer (Figure S1a). Excessive lead bromide ($PbBr_2$ powder, 99%, TCI Chemicals) and MABr powders are placed in the furnace at 350 °C in the upper stream of Ar flow (30 sccm, 100 Pa), while Si (100) or GaAs (100) wafers are placed in the down stream. The process lasts for ~20 min.

Materials Characterizations. X-ray diffraction (XRD) patterns are obtained with a Rigaku S2 diffractometer (40 kV, 40 mA). Phi scanning are performed using constant 2θ angles corresponding to the $MAPbBr_3$ (211) diffraction plane. XRD pole figures are measured using constant 2θ angles corresponding to the GaAs/PbS (111) planes and the $MAPbBr_3$ (211) plane. Asymmetric high-resolution reciprocal space maps (HR RSM) around (300) and (133) points of $MAPbBr_3$ are plotted with the scanning mode on a Bruker D8 Discover. Samples are placed with the GaAs cleavage direction ⟨110⟩ parallel to one side of the stage. SEM images are taken with a Zeiss GeminiSEM 500 (15 kV), and EBSD data are measured with a Zeiss Merlin. The EDS element mapping uses a sample prepared by a focused ion beam, milled, and transferred on a conductive bracket (electron voltage 15 kV). AFM images are obtained with a BRUKER Multimode 8 (peak-force tapping mode). Rutherford backscattering spectrometry (RBS) and channeling measurements are carried out using a 2 MeV $^4He^+$ beam from an accelerator at Peking University. Atomic structures were established with Materials Studio 8.0 (Accelrys).

■ ASSOCIATED CONTENT

Supporting Information

The Supporting Information is available free of charge at https://pubs.acs.org/doi/10.1021/acsami.2c15243.

$MAPbBr_3$ growth process via conventional CVD on Si and GaAs; cross-sectional HRTEM image; AFM data; and PL spectra (PDF)

■ AUTHOR INFORMATION

Corresponding Authors

Lan Yin − *School of Materials Science and Engineering, The Key Laboratory of Advanced Materials of Ministry of Education, State Key Laboratory of New Ceramics and Fine Processing, Center for Flexible Electronics Technology, Tsinghua University, Beijing 100084, China*; Email: lanyin@tsinghua.edu.cn

Xing Sheng − *Department of Electronic Engineering, Beijing National Research Center for Information Science and Technology, Center for Flexible Electronics Technology, IDG/*

https://doi.org/10.1021/acsami.2c15243
ACS Appl. Mater. Interfaces 2022, 14, 52508−52515

McGovern Institute for Brain Research, Tsinghua University, Beijing 100084, China; orcid.org/0000-0002-8744-1700; Email: xingsheng@tsinghua.edu.cn

Authors

Deying Kong − *School of Materials Science and Engineering, The Key Laboratory of Advanced Materials of Ministry of Education, State Key Laboratory of New Ceramics and Fine Processing, Center for Flexible Electronics Technology, Tsinghua University, Beijing 100084, China*

Yu Zhang − *Department of Physics, Tsinghua University, Beijing 100084, China*

Dali Cheng − *Department of Electronic Engineering, Beijing National Research Center for Information Science and Technology, Center for Flexible Electronics Technology, IDG/McGovern Institute for Brain Research, Tsinghua University, Beijing 100084, China*

Enze Wang − *School of Materials Science and Engineering, The Key Laboratory of Advanced Materials of Ministry of Education, State Key Laboratory of New Ceramics and Fine Processing, Center for Flexible Electronics Technology, Tsinghua University, Beijing 100084, China*

Kaiyuan Zhang − *Department of Electronic Engineering, Beijing National Research Center for Information Science and Technology, Center for Flexible Electronics Technology, IDG/McGovern Institute for Brain Research, Tsinghua University, Beijing 100084, China*

Huachun Wang − *Department of Electronic Engineering, Beijing National Research Center for Information Science and Technology, Center for Flexible Electronics Technology, IDG/McGovern Institute for Brain Research, Tsinghua University, Beijing 100084, China*

Kai Liu − *School of Materials Science and Engineering, The Key Laboratory of Advanced Materials of Ministry of Education, State Key Laboratory of New Ceramics and Fine Processing, Center for Flexible Electronics Technology, Tsinghua University, Beijing 100084, China;* orcid.org/0000-0002-0638-5189

Complete contact information is available at: https://pubs.acs.org/10.1021/acsami.2c15243

Notes

The authors declare no competing financial interest.

■ ACKNOWLEDGMENTS

This work is supported by the Tsinghua University Initiative Scientific Research Program, the State Key Laboratory of New Ceramic and Fine Processing Tsinghua University (KF202108), Beijing Municipal Natural Science Foundation (4202032), National Natural Science Foundation of China (NSFC) (52171239, T2122010, 52272277).

■ REFERENCES

(1) Cho, H.; Jeong, S.-H.; Park, M.-H.; Kim, Y.-H.; Wolf, C.; Lee, C.-L.; Heo, J. H.; Sadhanala, A.; Myoung, N.; Yoo, S.; Im, S. H.; Friend, R. H.; Lee, T.-W. Overcoming the Electroluminescence Efficiency Limitations of Perovskite Light-Emitting Diodes. *Science* **2015**, *350* (6265), 1222−1225.

(2) Dou, L.; Yang, Y.; You, J.; Hong, Z.; Chang, W.-H.; Li, G.; Yang, Y. Solution-Processed Hybrid Perovskite Photodetectors with High Detectivity. *Nat. Commun.* **2014**, *5* (1), 5404.

(3) Li, X.; Bi, D.; Yi, C.; Décoppet, J.-D.; Luo, J.; Zakeeruddin, S. M.; Hagfeldt, A.; Grätzel, M. A Vacuum Flash-Assisted Solution Process for High-Efficiency Large-Area Perovskite Solar Cells. *Science* **2016**, *353* (6294), 58−62.

(4) Chen, Q.; Wu, J.; Ou, X.; Huang, B.; Almutlaq, J.; Zhumekenov, A. A.; Guan, X.; Han, S.; Liang, L.; Yi, Z.; Li, J.; Xie, X.; Wang, Y.; Li, Y.; Fan, D.; Teh, D. B. L.; All, A. H.; Mohammed, O. F.; Bakr, O. M.; Wu, T.; Bettinelli, M.; Yang, H.; Huang, W.; Liu, X. All-Inorganic Perovskite Nanocrystal Scintillators. *Nature* **2018**, *561* (7721), 88−93.

(5) Akkerman, Q. A.; Rainò, G.; Kovalenko, M. V.; Manna, L. Genesis, Challenges and Opportunities for Colloidal Lead Halide Perovskite Nanocrystals. *Nat. Mater.* **2018**, *17* (5), 394−405.

(6) Saidaminov, M. I.; Abdelhady, A. L.; Murali, B.; Alarousu, E.; Burlakov, V. M.; Peng, W.; Dursun, I.; Wang, L.; He, Y.; Maculan, G.; Goriely, A.; Wu, T.; Mohammed, O. F.; Bakr, O. M. High-Quality Bulk Hybrid Perovskite Single Crystals within Minutes by Inverse Temperature Crystallization. *Nat. Commun.* **2015**, *6*, 7586.

(7) Chen, J.; Morrow, D. J.; Fu, Y.; Zheng, W.; Zhao, Y.; Dang, L.; Stolt, M. J.; Kohler, D. D.; Wang, X.; Czech, K. J.; Hautzinger, M. P.; Shen, S.; Guo, L.; Pan, A.; Wright, J. C.; Jin, S. Single-Crystal Thin Films of Cesium Lead Bromide Perovskite Epitaxially Grown on Metal Oxide Perovskite ($SrTiO_3$). *J. Am. Chem. Soc.* **2017**, *139* (38), 13525−13532.

(8) Zou, Y.; Li, F.; Zhao, C.; Xing, J.; Yu, Z.; Yu, W.; Guo, C. Anomalous Ambipolar Phototransistors Based on All-Inorganic $CsPbBr_3$ Perovskite at Room Temperature. *Adv. Opt. Mater.* **2019**, *7* (21), 1900676.

(9) Wang, L.; King, I.; Chen, P.; Bates, M.; Lunt, R. R. Epitaxial and Quasiepitaxial Growth of Halide Perovskites: New Routes to High End Optoelectronics. *APL Mater.* **2020**, *8* (10), 100904.

(10) Chen, J.; Zhou, Y.; Fu, Y.; Pan, J.; Mohammed, O. F.; Bakr, O. M. Oriented Halide Perovskite Nanostructures and Thin Films for Optoelectronics. *Chem. Rev.* **2021**, *121* (20), 12112−12180.

(11) Lei, Y.; Chen, Y.; Zhang, R.; Li, Y.; Yan, Q.; Lee, S.; Yu, Y.; Tsai, H.; Choi, W.; Wang, K.; Luo, Y.; Gu, Y.; Zheng, X.; Wang, C.; Wang, C.; Hu, H.; Li, Y.; Qi, B.; Lin, M.; Zhang, Z.; Dayeh, S. A.; Pharr, M.; Fenning, D. P.; Lo, Y.-H.; Luo, J.; Yang, K.; Yoo, J.; Nie, W.; Xu, S. A Fabrication Process for Flexible Single-Crystal Perovskite Devices. *Nature* **2020**, *583* (7818), 790−795.

(12) Chen, Y.; Lei, Y.; Li, Y.; Yu, Y.; Cai, J.; Chiu, M. H.; Rao, R.; Gu, Y.; Wang, C.; Choi, W.; Hu, H.; Wang, C.; Li, Y.; Song, J.; Zhang, J.; Qi, B.; Lin, M.; Zhang, Z.; Islam, A. E.; Maruyama, B.; Dayeh, S.; Li, L. J.; Yang, K.; Lo, Y. H.; Xu, S. Strain Engineering and Epitaxial Stabilization of Halide Perovskites. *Nature* **2020**, *577* (7789), 209−215.

(13) Lei, Y.; Chen, Y.; Gu, Y.; Wang, C.; Huang, Z.; Qian, H.; Nie, J.; Hollett, G.; Choi, W.; Yu, Y.; Kim, N.; Wang, C.; Zhang, T.; Hu, H.; Zhang, Y.; Li, X.; Li, Y.; Shi, W.; Liu, Z.; Sailor, M. J.; Dong, L.; Lo, Y. H.; Luo, J.; Xu, S. Controlled Homoepitaxial Growth of Hybrid Perovskites. *Adv. Mater.* **2018**, *30* (20), 1705992.

(14) Zhang, L.; Liu, L.; Zhang, P.; Li, R.; Zhang, G.; Tao, X. Thickness-Controlled Wafer-Scale Single-Crystalline $MAPbBr_3$ Films Epitaxially Grown on $CsPbBr_3$ Substrates by the Droplet-Evaporated Crystallization Method. *ACS Appl. Mater. Interfaces* **2020**, *12* (35), 39834−39840.

(15) Ji, L.; Hsu, H. Y.; Lee, J. C.; Bard, A. J.; Yu, E. T. High-Performance Photodetectors Based on Solution-Processed Epitaxial Grown Hybrid Halide Perovskites. *Nano Lett.* **2018**, *18* (2), 994−1000.

(16) Jiang, J.; Sun, X.; Chen, X.; Wang, B.; Chen, Z.; Hu, Y.; Guo, Y.; Zhang, L.; Ma, Y.; Gao, L.; et al. Carrier Lifetime Enhancement in Halide Perovskite via Remote Epitaxy. *Nat. Commun.* **2019**, *10* (1), 4145.

(17) Fan, C.; Xu, X.; Yang, K.; Jiang, F.; Wang, S.; Zhang, Q. Controllable Epitaxial Growth of Core-Shell $PbSe@CsPbBr_3$ Wire Heterostructures. *Adv. Mater.* **2018**, *30* (45), 1804707.

(18) Sytnyk, M.; Yousefi-Amin, A.-A.; Freund, T.; Prihoda, A.; Götz, K.; Unruh, T.; Harreiss, C.; Will, J.; Spiecker, E.; Levchuk, J.; Osvet, A.; Brabec, C. J.; Künecke, U.; Wellmann, P.; Volobuev, V. V.; Korczak, J.; Szczerbakow, A.; Story, T.; Simbrunner, C.; Springholz, G.; Wechsler, D.; Lytken, O.; Lotter, S.; Kampmann, F.; Maultzsch, J.; Singh, K.; Voznyy, O.; Heiss, W. Epitaxial Metal Halide Perovskites by Inkjet-Printing on Various Substrates. *Adv. Funct. Mater.* **2020**, *30* (43), 2004612.

(19) Zhong, Y.; Liao, K.; Du, W.; Zhu, J.; Shang, Q.; Zhou, F.; Wu, X.; Sui, X.; Shi, J.; Yue, S.; Wang, Q.; Zhang, Y.; Zhang, Q.; Hu, X.; Liu, X. Large-Scale Thin $CsPbBr_3$ Single-Crystal Film Grown on Sapphire via Chemical Vapor Deposition: Toward Laser Array Application. *ACS Nano* **2020**, *14* (11), 15605−15615.
(20) Geng, X.; Wang, F.; Tian, H.; Feng, Q.; Zhang, H.; Liang, R.; Shen, Y.; Ju, Z.; Gou, G. Y.; Deng, N.; Li, Y. T.; Ren, J.; Xie, D.; Yang, Y.; Ren, T. L. Ultrafast Photodetector by Integrating Perovskite Directly on Silicon Wafer. *ACS Nano* **2020**, *14* (3), 2860−2868.
(21) Zhao, L.; Gao, Y.; Su, M.; Shang, Q.; Liu, Z.; Li, Q.; Wei, Q.; Li, M.; Fu, L.; Zhong, Y.; Shi, J.; Chen, J.; Zhao, Y.; Qiu, X.; Liu, X.; Tang, N.; Xing, G.; Wang, X.; Shen, B.; Zhang, Q. Vapor-Phase Incommensurate Heteroepitaxy of Oriented Single-Crystal $CsPbBr_3$ on GaN: Toward Integrated Optoelectronic Applications. *ACS Nano* **2019**, *13* (9), 10085−10094.
(22) Li, Y.; Wang, X.; Wu, S.; Ci, H.; Xu, H.; Li, X.; Sun, H.; Zhang, Z.; Cao, A.; Guo, X.; Li, Y. Large-Scale Aligned Crystalline $CH_3NH_3PbI_3$ Perovskite Array Films. *J. Mater. Chem. A* **2015**, *3* (37), 18847−18851.
(23) Hill, J. C.; Koza, J. A.; Switzer, J. A. Electrodeposition of Epitaxial Lead Iodide and Conversion to Textured Methylammonium Lead Iodide Perovskite. *ACS Appl. Mater. Interfaces* **2015**, *7* (47), 26012−6.
(24) Kelso, M. V.; Mahenderkar, N. K.; Chen, Q.; Tubbesing, J. Z.; Switzer, J. A. Spin Coating Epitaxial Films. *Science* **2019**, *364* (6436), 166−169.
(25) Wang, Y.; Wan, Z.; Qian, Q.; Liu, Y.; Kang, Z.; Fan, Z.; Wang, P.; Wang, Y.; Li, C.; Jia, C.; Lin, Z.; Guo, J.; Shakir, I.; Goorsky, M.; Duan, X.; Zhang, Y.; Huang, Y.; Duan, X. Probing Photoelectrical Transport in Lead Halide Perovskites with van der Waals Contacts. *Nat. Nanotechnol.* **2020**, *15* (9), 768−775.
(26) Chen, J.; Luo, Z.; Fu, Y.; Wang, X.; Czech, K. J.; Shen, S.; Guo, L.; Wright, J. C.; Pan, A.; Jin, S. Tin(IV)-Tolerant Vapor-Phase Growth and Photophysical Properties of Aligned Cesium Tin Halide Perovskite ($CsSnX_3$; X = Br, I) Nanowires. *ACS Energy Lett.* **2019**, *4* (5), 1045−1052.
(27) Chen, J.; Fu, Y.; Samad, L.; Dang, L.; Zhao, Y.; Shen, S.; Guo, L.; Jin, S. Vapor-Phase Epitaxial Growth of Aligned Nanowire Networks of Cesium Lead Halide Perovskites ($CsPbX_3$, X = Cl, Br, I). *Nano Lett.* **2017**, *17* (1), 460−466.
(28) Chen, Z.; Dong, Q.; Liu, Y.; Bao, C.; Fang, Y.; Lin, Y.; Tang, S.; Wang, Q.; Xiao, X.; Bai, Y.; et al. Thin Single Crystal Perovskite Solar Cells to Harvest below-Bandgap Light Absorption. *Nat. Commun.* **2017**, *8* (1), 1890.
(29) Gu, Z.; Huang, Z.; Li, C.; Li, M.; Song, Y. A General Printing Approach for Scalable Growth of Perovskite Single-Crystal Films. *Sci. Adv.* **2018**, *4* (6), 2390.
(30) Lv, Q.; Lian, Z.; He, W.; Sun, J.-L.; Li, Q.; Yan, Q. A Universal Top-Down Approach Toward Thickness-Controllable Perovskite Single-Crystalline Thin Films. *J. Mater. Chem. C* **2018**, *6* (16), 4464−4470.
(31) Chen, C.; Hu, X.; Lu, W.; Chang, S.; Shi, L.; Li, L.; Zhong, H.; Han, J.-B. Elucidating the Phase Transitions and Temperature-Dependent Photoluminescence of $MAPbBr_3$ Single Crystal. *J. Phys. D: Appl. Phys.* **2018**, *51* (4), 045105.
(32) Wang, Y.; Shi, Y.; Xin, G.; Lian, J.; Shi, J. Two-Dimensional van der Waals Epitaxy Kinetics in a Three-Dimensional Perovskite Halide. *Cryst. Growth Des.* **2015**, *15* (10), 4741−4749.
(33) Adesida, I.; Agarwala, S.; Caneau, C.; Bhat, R. Highly Selective Etching of InGaAs on InAlAs in HBr Plasma. *Int. Conf. Indium Phosphide Relat. Mater.* **1993**, 529−532.
(34) Krueger, C. W.; Wang, C. A.; Flytzani-Stephanopoulos, M. Vapor Etching of GaAs and AlGaAs by CH_3I. *Appl. Phys. Lett.* **1992**, *60* (12), 1459−1461.
(35) Luo, Y.-R.*Comprehensive Handbook of Chemical Bond Energies*; CRC Press: Boca Raton, 2007; pp 1070 and 1403.
(36) Osherov, A.; Ezersky, V.; Golan, Y. The Role of Solution Composition in Chemical Bath Deposition of Epitaxial Thin Films of PbS on GaAs(100). *J. Cryst. Growth* **2007**, *308* (2), 334−339.
(37) Murza, V.; Friedman, O.; Vradman, L.; Golan, Y. Liquid Flow Deposition of PbS Films on GaAs(100). *CrystEngComm* **2018**, *20* (26), 3765−3771.
(38) Luo, P.; Zhou, S.; Liu, Z.; Xia, W.; Sun, L.; Cheng, J.; Xu, C.; Lu, Y. A Novel Transformation Route From PbS to $CH_3NH_3PbI_3$ for Fabricating Curved and Large-Area Perovskite Films. *Chem. Commun.* **2016**, *52* (75), 11203−11206.
(39) Perez, M.; Peled, S. S.; Templeman, T.; Osherov, A.; Bulovic, V.; Katz, E. A.; Golan, Y. All Solution Process for Conversion of Lead Sulfide to Methylammonium Lead Iodide Perovskite Thin Films. *Thin Solid Films* **2020**, *714*, 138367.
(40) Ning, Z.; Gong, X.; Comin, R.; Walters, G.; Fan, F.; Voznyy, O.; Yassitepe, E.; Buin, A.; Hoogland, S.; Sargent, E. H. Quantum-Dot-in-Perovskite Solids. *Nature* **2015**, *523* (7560), 324−8.
(41) Masi, S.; Echeverría-Arrondo, C.; Salim, K. M. M.; Ngo, T. T.; Mendez, P. F.; López-Fraguas, E.; Macias-Pinilla, D. F.; Planelles, J.; Climente, J. I.; Mora-Seró, I. Chemi-Structural Stabilization of Formamidinium Lead Iodide Perovskite by Using Embedded Quantum Dots. *ACS Energy Lett.* **2020**, *5* (2), 418−427.
(42) Toso, S.; Imran, M.; Mugnaioli, E.; Moliterni, A.; Caliandro, R.; Schrenker, N. J.; Pianetti, A.; Zito, J.; Zaccaria, F.; Wu, Y.; et al. Halide Perovskites as Disposable Epitaxial Templates for the Phase-Selective Synthesis of Lead Sulfochloride Nanocrystals. *Nat. Commun.* **2022**, *13* (1), 3976.
(43) Li, X. W.; Gupta, A.; Xiao, G.; Gong, G. Q. Transport and Magnetic Properties of Epitaxial and Polycrystalline Magnetite Thin Films. *J. Appl. Phys.* **1998**, *83* (11), 7049−7051.
(44) Visinoiu, A.; Alexe, M.; Lee, H. N.; Zakharov, D. N.; Pignolet, A.; Hesse, D.; Gösele, U. Initial Growth Stages of Epitaxial $BaTiO_3$ Films on Vicinal $SrTiO_3$ (001) Substrate Surfaces. *J. Appl. Phys.* **2002**, *91* (12), 10157−10162.
(45) Rideout, V. L. An Improved Polishing Technique for GaAs. *J. Electrochem. Soc.* **1972**, *119* (12), 1778.
(46) Han, J.; Luo, S.; Yin, X.; Zhou, Y.; Nan, H.; Li, J.; Li, X.; Oron, D.; Shen, H.; Lin, H. Hybrid PbS Quantum-Dot-in-Perovskite for High-Efficiency Perovskite Solar Cell. *Small* **2018**, *14*, 1801016.
(47) Osherov, A.; Ezersky, V.; Golan, Y. Hetero-Twinning in Chemical Epitaxy of PbS Thin Films on GaAs Substrates. *Cryst. Growth Des.* **2012**, *12* (8), 4006−4011.
(48) Meng, F.; Morin, S. A.; Jin, S., Growth of Nanomaterials by Screw Dislocation. In *Springer Handbook of Nanomaterials*; Vajtai, R., Ed.; Springer: Berlin, 2013; pp 639−664.
(49) Liu, M.; Chen, Y.; Tan, C.-S.; Quintero-Bermudez, R.; Proppe, A. H.; Munir, R.; Tan, H.; Voznyy, O.; Scheffel, B.; Walters, G.; Kam, A. P. T.; Sun, B.; Choi, M.-J.; Hoogland, S.; Amassian, A.; Kelley, S. O.; García de Arquer, F. P.; Sargent, E. H. Lattice Anchoring Stabilizes Solution-Processed Semiconductors. *Nature* **2019**, *570* (7759), 96−101.
(50) Deal, B. E.; Grove, A. S. General Relationship for the Thermal Oxidation of Silicon. *J. Appl. Phys.* **1965**, *36* (12), 3770−3778.
(51) Younis, A.; Hu, L.; Sharma, P.; Lin, C.-H.; Mi, Y.; Guan, X.; Zhang, D.; Wang, Y.; He, T.; Liu, X.; Shabbir, B.; Huang, S.; Seidel, J.; Wu, T. Enhancing Resistive Switching Performance and Ambient Stability of Hybrid Perovskite Single Crystals via Embedding Colloidal Quantum Dots. *Adv. Funct. Mater.* **2020**, *30* (31), 2002948.

https://doi.org/10.1021/acsami.2c15243
ACS Appl. Mater. Interfaces 2022, 14, 52508−52515

Supporting Information

Heteroepitaxy of Large-Area, Monocrystalline Lead Halide Perovskite Films on Gallium Arsenide

Deying Kong[a], Yu Zhang[b], Dali Cheng[c], Enze Wang[a], Kaiyuan Zhang[c], Huachun Wang[c], Kai Liu[a], Lan Yin,[a]* and Xing Sheng,[c]*

[a]*School of Materials Science and Engineering, The Key Laboratory of Advanced Materials of Ministry of Education, State Key Laboratory of New Ceramics and Fine Processing, Center for Flexible Electronics Technology, Tsinghua University, Beijing, 100084, China*

[b]*Department of Physics, Tsinghua University, Beijing, 100084, China*

[c]*Department of Electronic Engineering, Beijing National Research Center for Information Science and Technology, Center for Flexible Electronics Technology, IDG/McGovern Institute for Brain Research, Tsinghua University, Beijing, 100084, China*

*E-mail: lanyin@tsinghua.edu.cn (L. Y.)
*E-mail: xingsheng@tsinghua.edu.cn (X. S.)

Additional experimental details, materials, and methods (Supplementary Figures S1–S4)

Figure S1

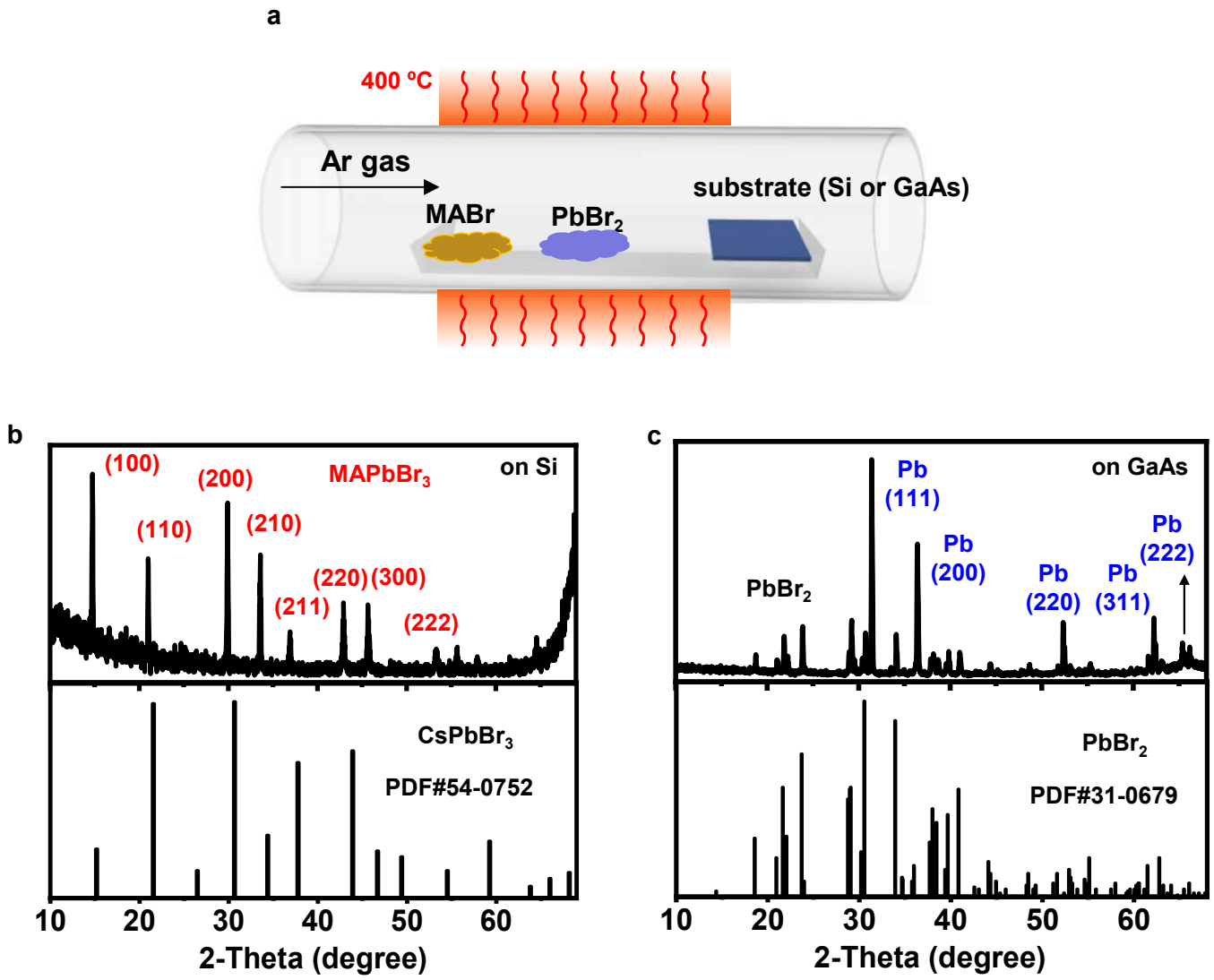

Figure S1. (a) $MAPbBr_3$ growth via conventional CVD, by reacting MABr and $PbBr_2$ on Si or GaAs at 400 ºC in argon environment. (b) XRD pattern for the CVD deposited film on Si, indicating the formation of polycrystalline $MAPbBr_3$. (c) XRD pattern for the CVD deposited film on GaAs, indicating the formation of polycrystalline $PbBr_2$ and Pb, but no $MAPbBr_3$. Powder Diffraction Files (PDF) of $CsPbBr_3$ and $PbBr_2$ are provided for comparison.

Figure S2

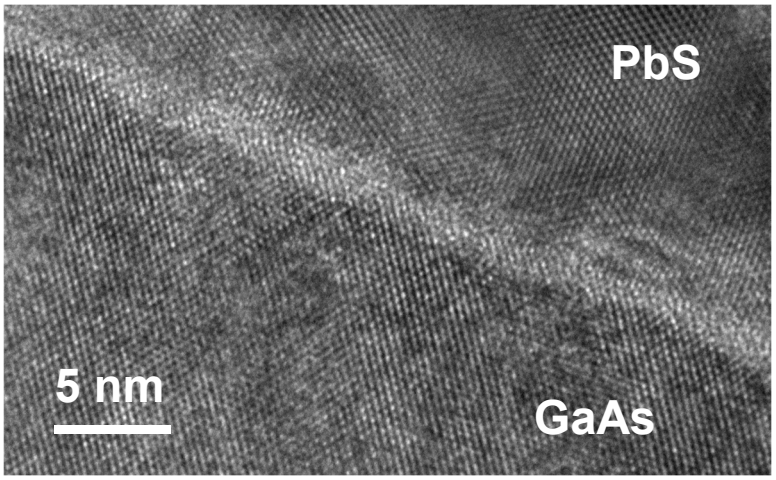

Figure S2. Cross-sectional high-resolution transmission electron microscopic (HRTEM) of the PbS/GaAs interface.

Figure S3

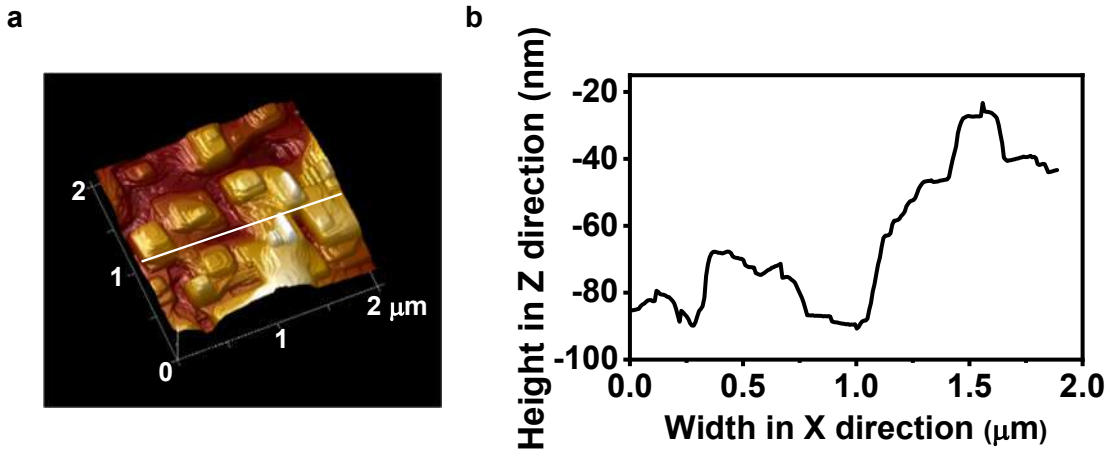

Figure S3. (a) AFM of the $MAPbBr_3$ film grown on PbS/GaAs for 8 hours, (b) 1D scan showing the maximum roughness.

Figure S4

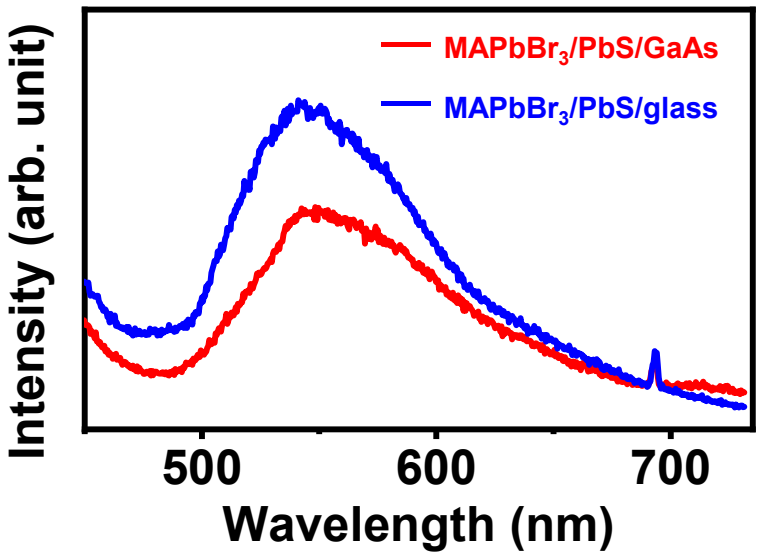

Figure S4. Photoluminescence spectra for $MAPbBr_3$ films grown on PbS/GaAs (red) and PbS/glass (blue). The excitation source is a 365 nm LED.